engineering proceedings

MDPI

Proceeding Paper

Experimental and Numerical Study of Mode II Fatigue Delamination via End-Loaded Split Specimens †

Johan Birnie *, Maria Pia Falaschetti, Francesco Semprucci and Enrico Troiani

MaSTeR Lab, Department of Industrial Engineering, University of Bologna, Via Fontanelle 40, 47121 Forlì, FC, Italy; mariapi.falaschetti2@unibo.it (M.P.F.); francesco.semprucci2@unibo.it (F.S.); enrico.troiani@unibo.it (E.T.)

* Correspondence: johan.birnie2@unibo.it

† Presented at the 8th International Conference of Engineering Against Failure (ICEAF VIII), Kalamata, Greece, 22–25 June 2025.

Abstract

Delamination in fibre-reinforced polymer composites is a critical failure mechanism that can ultimately lead to a catastrophic failure. To characterise in-plane shear delamination (Mode II), several test setups have been proposed in the literature, with the End-Loaded Split (ELS) test being the most suitable for applications that require stable crack propagation (ISO 15114). This manuscript focuses on studying Mode II fatigue delamination in unidirectional carbon fibre-reinforced laminates using the ELS configuration. Experimental tests with varying displacement ratios and different initial energy levels were conducted to capture a wide range of stable crack propagation scenarios. To complement these experimental efforts, a numerical model based on cohesive zone models (CZM) was implemented in Abaqus, utilising a user-defined material subroutine (UMAT). The numerical results closely align with the experimental data, validating the model's predictive capabilities. This combined approach deepens the understanding of Mode II fatigue delamination and provides a strong framework for designing and analysing composite structures.

Keywords: ELS; Mode II; delamination; fatigue; cohesive zone models

check for updates

Academic Editors: Spiros Pantelakis and Spyros Diplas

Published: 7 January 2026

Citation: Birnie, J.; Falaschetti, M.P.; Semprucci, F.; Troiani, E. Experimental and Numerical Study of Mode II Fatigue Delamination via End-Loaded Split Specimens. *Eng. Proc.* **2025**, *119*, 50. https://doi.org/10.3390/engproc2025119050

Copyright: © 2026 by the authors. Licensee MDPI, Basel, Switzerland. This article is an open access article distributed under the terms and conditions of the Creative Commons Attribution (CC BY) license (https://creativecommons.org/licenses/by/4.0/).

1. Introduction

Delamination is a major failure mechanism in composite materials, typically initiated by excessive out-of-plane or interlaminar stresses, which leads to stiffness degradation and ultimately structural failure [1]. In fracture mechanics, delamination is generally classified into three damage modes: Mode I (tensile opening), Mode II (in-plane shear), and Mode III (transverse shear). However, real-world structures rarely exhibit these pure delamination modes; instead, they often experience a combination of them (i.e., Mixed-Mode), primarily a combination of Mode I and Mode II.

Despite this, mixed-mode criteria still rely on pure fracture modes. In the literature, the Double Cantilever Beam (DCB) specimen has been widely used for the study of Mode I delamination. In contrast, reliable characterisation of Mode II delamination remains challenging due to unstable crack propagation and difficulties in visually evaluating the crack length in Mode II. This results in the proposal of various testing setups, among which are the End-Notched Flexure (ENF), the End-Loaded Split (ELS), the 4-point bending End-Notched Flexure (4ENF), and the Central Cut Ply (CCP) tests [2]. To determine the Mode II fracture toughness of unidirectional fibre-reinforced polymer matrix composites (FRPs), ASTM has published the D-7905 standard, which utilises the ENF specimen [3].

Meanwhile, the International Organization for Standardization (ISO) has proposed the ISO-15114 standard featuring the ELS [4].

Utilising the ASTM standardised test, it is possible to obtain only the initiation values of the Mode II fracture toughness (G_{IIC}) due to unstable crack propagation. Conversely, the ISO test employing the ELS, despite introducing some variabilities due to clamping differences, allows for stable crack propagation and, therefore, is suitable for studying fatigue crack growth [5,6].

This study investigates Mode II fatigue delamination in unidirectional Carbon FRP laminates using the ELS configuration, as performed by Pirondi and Moroni [7] on bonded joints. Experimental testing is complemented by a numerical simulation framework based on Cohesive Zone Models (CZMs). CZMs employ Finite Element Modelling (FEM) techniques to model the interlaminar interface. Damage initiation and evolution are governed by the constitutive laws of the cohesive interface, applicable for both static and fatigue loading. Specifically, this study used the high-cycle fatigue model proposed by Turon et al. [8].

By integrating the experimental results with validated simulations, this study seeks to improve the understanding of the fatigue behaviour of Mode II delamination, thereby aiding in the predictive modelling of composite structures subjected to cyclic loading.

2. Materials and Methods

2.1. Specimen's Material and Manufacturing

The carbon fibre-reinforced polymer (CFRP) laminates used for this study were manufactured from T700-300-DT120 (300 gsm) epoxy prepreg from Delta Preg S.p.A. (Sant'Egidio alla Vibrata, Italy) with a $[0]_{10}$ stacking sequence. The mechanical properties of the laminate are summarised in Table 1 [9].

Table 1. Elastic properties of the CFRP T700-DT120.

Properties	Symbol	Value	Units
Longitudinal Modulus	E_{11}	132	GPa
Transverse Modulus	E_{22}	14.5	GPa
Poisson's Ratio	ν_{12}	0.295	-
Shear Modulus	G_{12}	4.95	GPa

An artificial delamination crack in the mid-plane was introduced during the hand lay-up with a 25 µm thick and 70 mm long Ethylene tetrafluoroethylene (ETFE) film insert. Specimens were cut out of the 3.10 mm-thick cured panel with dimensions of 214 × 20 mm. Additionally, a 20 × 15 mm loading block was glued to the pre-cracked side, as illustrated in Figure 1. A constrained Mode I pre-cracking procedure was performed to remove any resin-rich areas at the interface between the film insert and the resin.

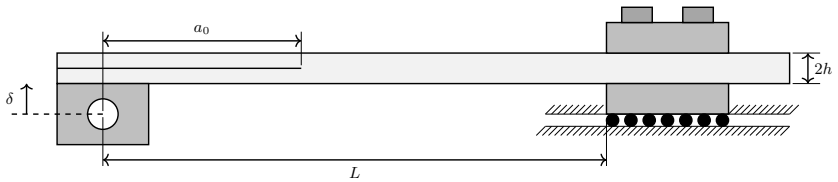

Figure 1. ELS test scheme: specimen's geometry, clamping fixture and loading point.

2.2. Test Set-Up

The specimen's geometry and fixture met the specifications suggested on the ISO-15114 standard [4]. Figure 1 illustrates the specimen, loading block, and clamp. Important geometrical parameters are also illustrated with the loading point (δ), the initial crack

length (a_0) measured from the loading point to the crack tip, the thickness of the specimen ($2h$), and the free length (L) measured from the loading point to the clamp border. Testing was carried out in an MTS 831 Elastomer Test System (Eden Prairie, MN, USA) with a 10 kN load capacity under displacement control with a 500 N load cell.

2.2.1. Static Tests

Five specimens were tested under static loading conditions to determine the Mode II fracture toughness (G_{IIC}). The characteristics of the tested specimens at the free length (L) of 105 mm are summarised in Table 2. Each specimen was loaded at a displacement rate of 0.5 mm/min, and the test was stopped once the crack had fully propagated. According to the ISO standard, for stable propagation, the condition $a_0/L > 0.55$ shall be met.

Table 2. Visually measured initial crack length and (a_0/L) ratio of the tested specimens under static loading.

Specimen	Initial Crack Length (a_0) [mm]	a_0/L
ELS_03	75	0.71
ELS_17	65	0.61
ELS_21	60	0.57
ELS_22	60	0.57
ELS_23	60	0.57

2.2.2. Fatigue Tests

Six specimens were tested under fatigue loading conditions by applying a sinusoidal waveform at a frequency of 2.5 Hz, with two different displacement ratios (R_d). The initial maximum displacement varied due to the reduced crack propagation area in the presence of the clamped end. Each specimen had an initial pre-cracked length of 65 mm, which was visually inspected. A summary of the testing conditions for each specimen is presented in Table 3.

Table 3. Fatigue testing conditions of the different specimens.

Specimen	R_d	Maximum Displacement [mm]	Number of Cycles
ELS_05	0.1	11.0	601,520
ELS_06		18.0	14,000
ELS_07		25.8	600
ELS_08	0.3	22.0	7,000
ELS_11		18.0	30,096
ELS_13		12.5	450,153

2.3. Data Reduction Methods

To determine the Mode II fracture toughness (G_{IIC}), the ISO-15114 standard outlines three distinct methods: Simple Beam Theory (SBT), Experimental Compliance Method (ECM), and Corrected Beam Theory with Effective Crack Length (CBTE). The first two methods rely on measuring the crack length during testing, whilst the CBTE calculates an effective crack length based on the compliance (C) along with the geometrical and physical parameters derived from the clamp calibration test. This manuscript will focus exclusively on the CBTE method. The effective crack length (a_e) is calculated as follows:

$$a_e = \left[\frac{1}{3}\left\{2bCh^3E_{flex} - \left(L + \Delta_{clamp}\right)^3\right\}\right]^{\frac{1}{3}}, \quad (1)$$

where b is the specimen's width, E_{flex} is the flexural modulus, and Δ_{clamp} is the clamping correction. The last two parameters come from the clamp calibration test, and for the tested specimens, they have a value of $E_{flex} = 131,288.24$ MPa, and $\Delta_{clamp} = 15.12$ mm.

The energy release rate for mode II is determined using Equation (2), and the corresponding R-curve can be plotted based on the output values. Large displacement and load-block effects were also taken into consideration.

$$G_{IIC} = \frac{9P^2a_e^2}{4b^2h^3E_{flex}}, \tag{2}$$

where P is the applied load. For fatigue crack propagation tests, the standard Paris' Law was used to describe the stable crack propagation, considering only the maximum strain energy release rate for Mode II ($G_{II_{max}}$) as in Equation (3).

$$\frac{da}{dN} = C_0 G_{II_{max}}^m, \tag{3}$$

where $\frac{da}{dN}$ is the crack propagation rate, and C_0 and m are material constants.

2.4. Finite Element Modelling

The FEM used to simulate the ELS specimen was developed in Abaqus/Standard 2024 using a 2D approach. The specimen was divided into two sublaminates, each with a thickness h, tied with a 0.001 mm-thick cohesive layer. The laminates' contact properties were a no-penetration in the normal direction and frictionless in the tangential direction. The initial crack length was analysed on a case-by-case basis. The laminates were modelled using CPE4I elements, whilst the cohesive layer was modelled with COH2D4 elements. The properties of the cohesive layer are summarised in Table 4.

Table 4. Cohesive properties of the CFRP T700-DT120.

Properties	Symbol	Value	Units
Normal Stiffness	K_n	6×10^6	N/mm^3
Tangential Stiffness	K_t	2.5×10^6	N/mm^3
Maximum Traction (Mode II)	τ_{II}^0	100	MPa
Fracture Toughness (Mode II)	G_{IIC}	2.5	N/mm

The clamped end was represented with a boundary condition that allows only horizontal displacement (sliding). The loading block was modelled using a multi-point constraint (MPC), allowing only vertical displacement and rotations. The described conditions are illustrated in Figure 2.

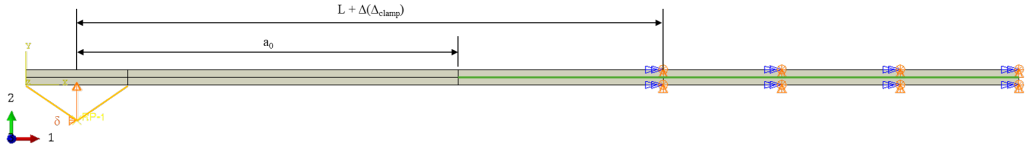

Figure 2. Visual representation of the modelled ELS with its boundary conditions. Sublaminates are represented in pale yellow, with the cohesive layer in green. $\Delta(\Delta_{clamp})$ represents the clamp correction between simulations and experiments.

Cohesive Zone Models

Commercially available FEM software lacks built-in features for simulating fatigue delamination. To address this limitation, an in-house user-defined material subroutine (UMAT) was implemented [10]. This UMAT governs the behaviour of cohesive elements

where delamination occurs, enabling the simulation of damage propagation under both static and fatigue loading conditions.

The implemented subroutine is based on the model proposed by Turon et al. [8], in which damage evolution is described by a traction-separation law, specifically a bi-linear traction law (BTSL). The BTSL features a linear elastic behaviour up to the critical cohesive strength, followed by a progressive reduction in the stiffness, reflecting the damage accumulation. The displacements of the cohesive elements drive this stiffness degradation, and the area under the BTSL curve corresponds to the fracture toughness (G_C).

The total damage (d) accounts for both static and fatigue loads. Under static loading, damage is a function of the relative displacements of the cohesive elements and may be computed with Equation (4).

$$d_{static} = \frac{\delta^f(r - \delta^0)}{\lambda(\delta^f - \delta^0)}, \tag{4}$$

where δ^0 is the onset displacement, δ^f is the propagation displacement, λ is the displacement jump, and r is the damage threshold.

On the other hand, for fatigue loading, the model considers only the maximum envelope of the cyclic loading history, employing a cycle jump strategy to update the damage value after a specified number of cycles, ΔN, as expressed in Equation (5). The fatigue damage growth in this particular model couples a delamination growth law $\frac{da}{dN}$ (i.e., the Paris Law) coming from experimental testing with the evolution of the damaged area $\frac{dd}{da}$, as expressed in Equation (6).

$$d^i_{fatigue} = d^{i-1}_{fatigue} + \frac{dd}{dN}\Delta N, \tag{5}$$

$$\frac{dd}{dN} = \frac{dd}{da}\frac{da}{dN}, \tag{6}$$

where i represents the current increment and $i - 1$ the previous increment.

3. Results and Discussion

3.1. Static Tests

The static loading results from the experimental tests were compared with the FEM numerical results, considering a crack length of 65 mm. As shown in Figure 3a, the force–displacement curves demonstrate a similar trend between the experimental and numerical results, although the differences in the slope are attributed to the different initial crack lengths of the tested specimens, due to the pre-cracking to remove any resin-rich areas at the crack front.

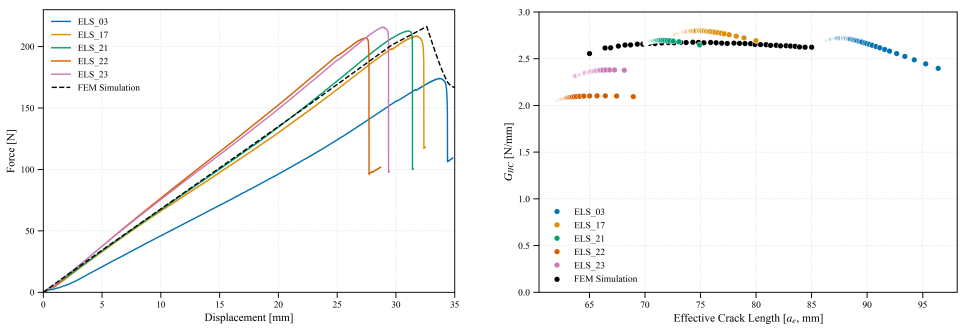

(a) (b)

Figure 3. Force–displacement curves (**a**) and R-curves (**b**) from different specimens with a free length of L = 105 mm.

Furthermore, the R-curves are presented in Figure 3b, highlighting stable crack propagation in all specimens for at least 5 mm. This feature was one of the reasons for selecting this particular setup. The numerical results show a good agreement with the experimental outcomes in terms of G_{IIC}.

The values for both the initiation and propagation fracture toughness from the experimental tests, which were then taken into consideration for the numerical model, are summarised in Table 5.

Table 5. Experimental values of G_{IIC} for five specimens. Initiation, critical, and propagation values are listed with their respective mean and standard deviation.

Specimen's Name	G_{IIC} [N/mm]		
	Initial	**Critical (max)**	**Propagation (mean)**
ELS_03	2.69	2.72	2.69
ELS_17	2.76	2.80	2.78
ELS_21	2.67	2.70	2.70
ELS_22	2.05	2.10	2.08
ELS_23	2.31	2.38	2.35
Mean Fracture Toughness	2.50 ± 0.30	2.54 ± 0.29	2.52 ± 0.29

3.2. Fatigue Tests

The fatigue loading results from the experimental tests were compared with the FEM numerical outcomes. The crack propagation rate against the maximum strain energy release rate is presented in Figure 4, where the trend of the numerical results is similar to those of the experimental tests.

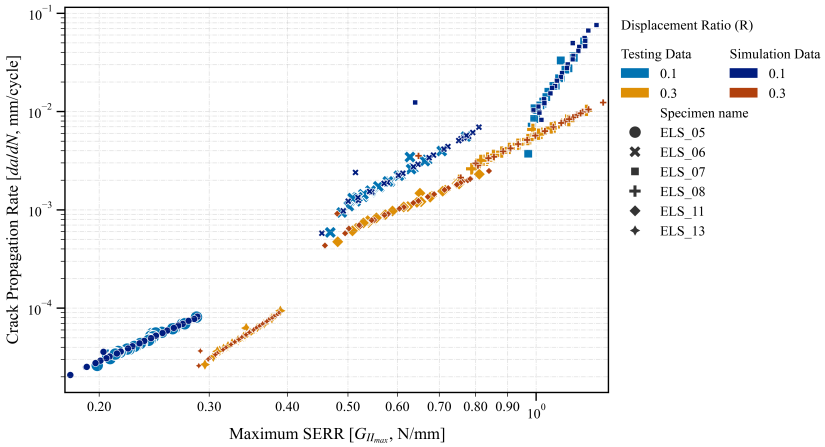

Figure 4. Experimental and numerical stable crack propagation rate: maximum strain energy release rate (SERR, $G_{II_{max}}$) for six specimens at two displacement ratios.

As mentioned in Section 2.2.2, the crack propagation area in the ELS test configuration is restricted due to the presence of a clamped end, which acts as a crack arrest feature. This limitation led to performing multiple tests at the same displacement ratio but with varying maximum displacements, thus introducing different initial energy levels. This approach enables the construction of a Paris curve that encompasses most of the stable propagation energy spectrum.

It is important to note that the slope for specimen ELS_07 exhibits the most significant deviation when compared to the others. This is because, at the specified energy level, the specimen did not transition into stable crack propagation. Instead, it exhibited high rates of crack propagation, which are characteristic of the unstable growth typically observed

during the initial phase of delamination. Furthermore, all the tested specimens exhibit a slight change in slope as the delamination propagates. This change is due to the influence of the clamped end, which alters the stress ratio at a constant displacement ratio. These effects are effectively captured by the numerical model, which utilises the experimental parameters from the Paris curve as an input.

Figure 5 illustrates a single curve based on the Paris Law, encompassing all the data with the same displacement ratio for both numerical and experimental approaches. The coefficients of the Paris Law, derived from fitting the power function described in Equation (3), are summarised in Table 6. All the fitted curves exhibit a correlation coefficient close to 1, indicating a strong fit between the data and the curve. Notably, the comparison of the m coefficients shows a maximum error of less than 4%, demonstrating a high level of accuracy in the implemented numerical model.

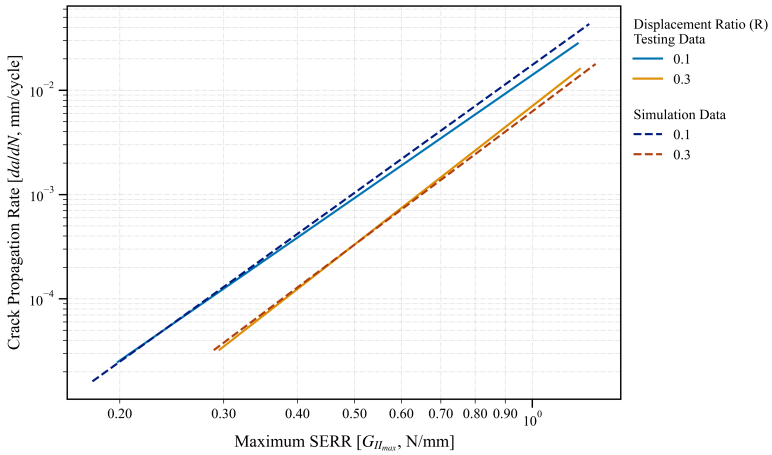

Figure 5. Experimental and numerical Paris curves, grouping results from different displacement ratios.

Table 6. Paris law coefficients from experimental and numerical curves from different displacement ratios with their respective coefficients of determination.

R_d		C_0	m	R^2	Error [%]
0.1	Tests	1.403×10^{-2}	3.919	0.994	3.88
	Simulation	1.749×10^{-2}	4.071	0.993	
0.3	Tests	7.060×10^{-3}	4.409	0.991	3.80
	Simulation	6.271×10^{-3}	4.241	0.987	

4. Conclusions

The ELS test setup has effectively demonstrated stable crack growth under both static and fatigue loads. The significance of conducting fatigue tests at various initial displacement levels has been highlighted to define a complete stable crack propagation region. Furthermore, it was identified that the stress ratio may vary as the delamination front approaches the clamped end, which may shift the results of each tested specimen.

The simulation outcomes confirm that the cohesive zone model accurately replicates the material behaviour observed experimentally under both static and fatigue conditions, thereby supporting its application in predictive modelling for delamination studies.

Future research efforts will concentrate on advanced crack tip tracking by utilising Digital Image Correlation (DIC) data from both side and top views, which will allow for comparison with alternative data reduction techniques. In addition, further investigation is required to develop a deeper understanding of the effects and failure mechanisms associated with varying displacement ratios.

Author Contributions: J.B.: Conceptualization, methodology, software, validation, formal analysis, investigation, data curation, writing—original draft preparation, writing—review and editing; M.P.F.: Methodology, visualization, writing—review and editing; F.S.: writing—original draft preparation, writing—review and editing; E.T.: Methodology, supervision, project administration, funding acquisition, writing—review and editing. All authors have read and agreed to the published version of the manuscript.

Funding: This research was funded by the European Union—NextGenerationEU through the Italian Ministry of University and Research under PNRR, Mission 4 Component 1, Investment 4.1 and 3.4; CUP: J33C23002650002.

Institutional Review Board Statement: Not applicable.

Informed Consent Statement: Not applicable.

Data Availability Statement: The datasets presented in this article are not readily available because the data are part of an ongoing study.

Acknowledgments: J. Birnie acknowledges the support of Delft University of Technology (TU Delft) during the testing campaign.

Conflicts of Interest: The authors declare no conflicts of interest.

References

1. Greenhalgh, E.S. 4—Delamination-dominated failures in polymer composites. In *Failure Analysis and Fractography of Polymer Composites*; Woodhead Publishing Series in Composites Science and Engineering; Woodhead Publishing: Cambridge, UK, 2009; pp. 164–237. [CrossRef]
2. Brunner, A.J.; Stelzer, S.; Pinter, G.; Terrasi, G.P. Mode II fatigue delamination resistance of advanced fiber-reinforced polymer–matrix laminates: Towards the development of a standardized test procedure. *Int. J. Fatigue* **2013**, *50*, 57–62. [CrossRef]
3. *ASTM D7905:2014*; Standard Test Method for Determination of the Mode II Interlaminar Fracture Toughness of Unidirectional Fiber-Reinforced Polymer Matrix Composites. American Society for Testing and Materials: West Conshohocken, PA, USA, 2014.
4. *ISO 15114:2014(E)*; Fibre-Reinforced Plastic Composites—Determination of the Mode II Fracture Resistance for Unidirectionally Reinforced Materials Using the Calibrated End-Loaded Split (c-ELS) Test and an Effective Crack Length Approach. ISO: Geneva, Switzerland, 2014.
5. Blackman, B.R.K.; Brunner, A.J.; Williams, J.G. Mode II fracture testing of composites: A new look at an old problem. *Eng. Fract. Mech.* **2006**, *73*, 2443–2455. [CrossRef]
6. Wang, H.; Vu-Khanh, T. Use of end-loaded-split (ELS) test to study stable fracture behaviour of composites under mode II loading. *Compos. Struct.* **1996**, *36*, 71–79. [CrossRef]
7. Pirondi, A.; Moroni, F. Simulation of Mixed-Mode I/II Fatigue Crack Propagation in Adhesive Joints with a Modified Cohesive Zone Model. *J. Adhes. Sci. Technol.* **2011**, *25*, 2483–2499. [CrossRef]
8. Turon, A.; Costa, J.; Camanho, P.P.; Dávila, C.G. Simulation of delamination in composites under high-cycle fatigue. *Compos. Part A: Appl. Sci. Manuf.* **2007**, *38*, 2270–2282. [CrossRef]
9. Falaschetti, M.P.; Rondina, F.; Zavatta, N.; Troiani, E.; Donati, L. Effective implementation of numerical models for the crashworthiness of composite laminates. *Eng. Fail. Anal.* **2024**, *160*, 108196. [CrossRef]
10. Birnie, J.; Falaschetti, M.P.; Troiani, E. Comparative Analysis on Modelling Approaches for the Simulation of Fatigue Disbonding with Cohesive Zone Models. *Aerospace* **2025**, *12*, 139. [CrossRef]

Disclaimer/Publisher's Note: The statements, opinions and data contained in all publications are solely those of the individual author(s) and contributor(s) and not of MDPI and/or the editor(s). MDPI and/or the editor(s) disclaim responsibility for any injury to people or property resulting from any ideas, methods, instructions or products referred to in the content.